PROTEINS: Structure, Function, and Genetics 7:74–92 (1990)

Structure Determination and Refinement of *Bacillus stearothermophilus* Lactate Dehydrogenase

Klaus Piontek,[1] Pinakpani Chakrabarti,[1] Hans-Peter Schär,[1] Michael G. Rossmann,[1] and Herbert Zuber[2]

[1]Department of Biological Sciences, Purdue University, West Lafayette, Indiana 47907; [2]Institut für Molekularbiologie and Biophysik, Eidgenössische Technische Hochschule-Hönggerberg, CH-8093 Zürich, Switzerland

ABSTRACT **Structures have been determined of *Bacillus stearothermophilus* "apo" and holo lactate dehydrogenase. The holo-enzyme had been co-crystallized with the activator fructose 1,6-bisphosphate. The "apo" lactate dehydrogenase structure was solved by use of the known apo-M_4 dogfish lactate dehydrogenase molecule as a starting model. Phases were refined and extended from 4 Å to 3 Å resolution by means of the noncrystallographic molecular 222 symmetry. The *R*-factor was reduced to 28.7%, using 2.8 Å resolution data, in a restrained least-squares refinement in which the molecular symmetry was imposed as a constraint. A low occupancy of coenzyme was found in each of the four subunits of the "apo"-enzyme.**

Further refinement proceeded with the isomorphous holo-enzyme from *Bacillus stearothermophilus*. After removing the noncrystallographic constraints, the *R*-factor dropped from 30.3% to a final value of 26.0% with a 0.019 Å and 1.7° r.m.s. deviation from idealized bond lengths and angles, respectively.

Two sulfate ions per subunit were included in the final model of the "apo"-form—one at the substrate binding site and one close to the molecular *P*-axis near the location of the fructose 1,6-bisphosphate activator. The final model of the holo-enzyme incorporated two sulfate ions per subunit, one at the substrate binding site and another close to the *R*-axis. One nicotinamide adenine dinucleotide coenzyme molecule per subunit and two fructose 1,6-bisphosphate molecules per tetramer were also included. The phosphate positions of fructose 1,6-bisphosphate are close to the sulfate ion near the *P*-axis in the "apo" model.

This structure represents the first reported refined model of an allosteric activated lactate dehydrogenase. The structure of the activated holo-enzyme showed far greater similarity to the ternary complex of dogfish M_4 lactate dehydrogenase with nicotinamide adenine dinucleotide and oxamate than to apo-M_4 dogfish lactate dehydrogenase. The conformations of nicotinamide adenine dinucleotide and fructose 1,6-bisphosphate were also analyzed.

Key words: thermostability, bacterial lactate dehydrogenase, allosteric regulation, crystallography, molecular replacement, coenzyme binding

INTRODUCTION

Lactate dehydrogenase (LDHase), an NAD-dependent redox enzyme, catalyzes the conversion of pyruvate to lactate in the last step of the anaerobic glycolytic pathway. In most organisms, the active form consists of four subunits, has a molecular weight of about 140,000 daltons, and exhibits 222 symmetry (for a review see Holbrook et al.[1]).

Several high resolution structures of apo-LDHase[2–5] as well as ternary[6,7] complexes from vertebrates have been solved. These studies revealed a movement of a loop segment (Fig. 1) over the active site when coenzyme and substrate are bound to the enzyme. The first 12–14 amino acids are deleted in LDHases from bacterial sources with respect to those from vertebrate LDHases.[8–10] It has been sug-

Received March 8, 1989; revision accepted August 9, 1989.

Address reprint requests to Michael G. Rossmann, Department of Biological Sciences, Purdue University, West Lafayette, IN 47907.

Klaus Piontek's present address is Lab. für Biochemie, ETH-Zentrum, CH-8093 Zürich, Switzerland.

Pinakpani Chatrabarti's present address is Division of Chemistry and Chemical Engineering, California Institute of Technology, Pasadena, CA 91125.

Hans-Peter Schär's present address is Central Research Laboratories of CIBA-GEIGY AG, CH-4002 Basel, Switzerland.

Abbreviations used: ADHase: alcohol dehydrogenase; BSLDHase: *Bacillus stearothermophilus* lactate dehydrogenase (the letter "a" preceding the abbreviated enzyme names refers to the apo-enzyme, the letters "h" and "t" refer to a holo-enzyme and ternary complex, respectively); DMLDHase: dogfish M_4 lactate dehydrogenase; FBP: D-fructose 1,6-bisphosphate; LADHase: liver alcohol dehydrogenase; LDHase: lactate dehydrogenase. "Apo" refers to the enzyme which was originally thought to be in the native form, but later turned out to be partially substituted with coenzyme.

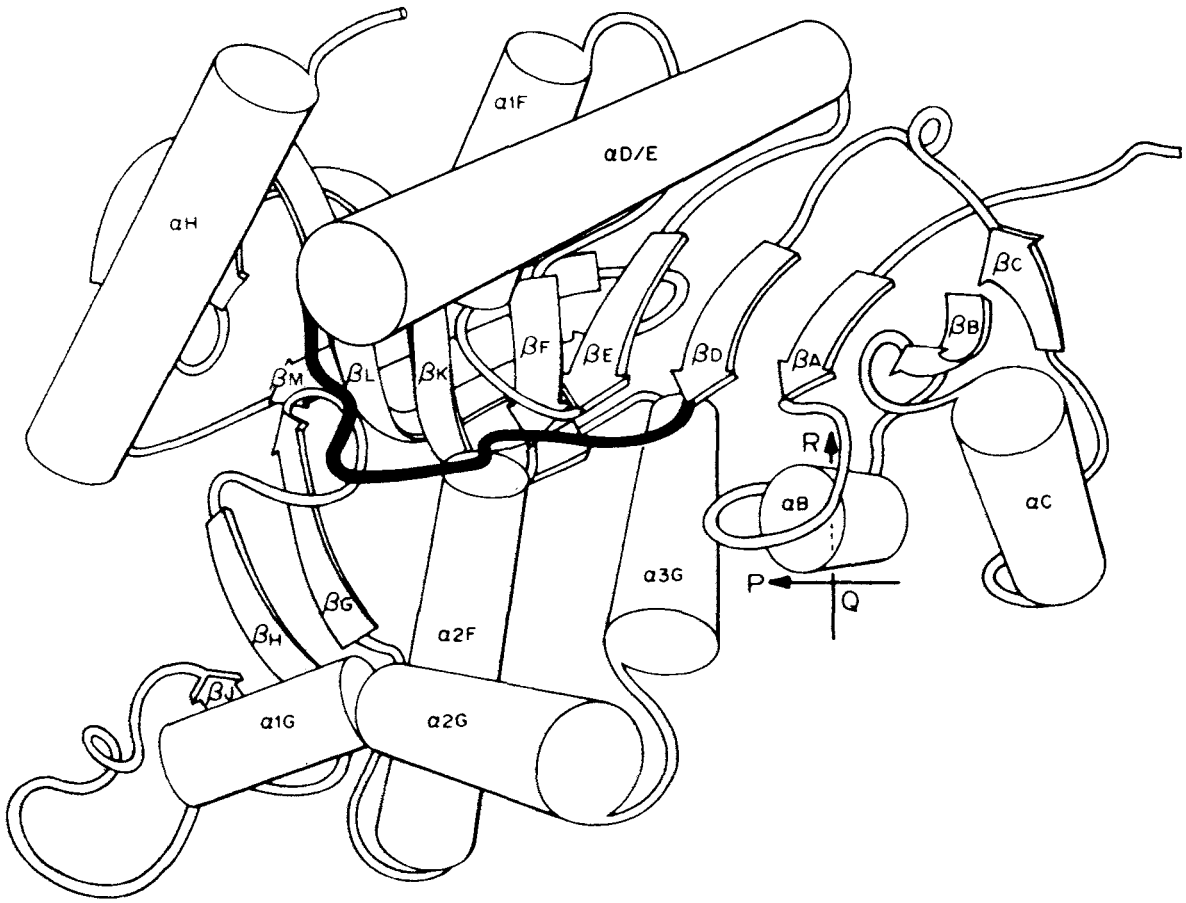

Fig. 1. Diagrammatic representation of the tertiary structure of hBSLDHase. The flexible loop is blackened.

gested that this N-terminal arm stabilizes the tetrameric quaternary structure.[1,11] Most bacterial LDHases are regulated by allosteric activators, such as FBP[8,12,13] and/or certain cations.[14,15] *B. stearothermophilus* belongs to a class of microorganisms which has enzymes that show higher thermostability than those from related mesophilic species.[16,17] Their enhanced thermal stability seems to be an inherent structural property.[18] The most studied microbial LDHase that is activated by FBP is that from *B. stearothermophilus*.[19] Its amino acid[20] and gene[21,22] sequences have been determined and much is known about its kinetic, ligand-binding, and quaternary structural properties.[8,20,23] Site-specific mutagenesis has permitted closer insight of some structurally and functionally important residues.[24–26]

BSLDHase has 35% of its amino acids identical to DMLDHase (Fig. 2).[20] The latter molecule was used here for molecular replacement as a start to the structure determination. In this paper we describe the structure determination and refinement of LDHase from *B. stearothermophilus*, thus representing the first refined model of a bacterial LDHase.

MATERIALS AND METHODS

The phase problem was solved with the data of the "apo" compound using the molecular replacement method based on initial phases from the known aDMLDHase structure.[3] The refined "apo" BSLDHase model was used later for the refinement of the isomorphous holo-form from BSLDHase.

Data Collection and Processing

Type 3 crystals of the "apo"- and type 4 crystals of the holo-form, described by Schär et al.,[28] were used in the structure determination of BSLDHase. The space group of both forms is $P6_1$, rather than $P6_122$ as originally reported. The unit cells have dimensions a = b = 86.9 Å, c = 357.3 Å for the "apo"-form and a = b = 86.8 Å, c = 356.6 Å for the holo-form. Each cell contains a complete tetramer with a molecular weight of 135,000 daltons per crystallographic asymmetric unit. The packing density, V_M, is 2.88 Å^3/dalton.[29]

Both crystal forms diffract to at least 2.5 Å resolution. The two data sets were collected with an Elliott GX6 rotating anode tube, operated at 35 kV,

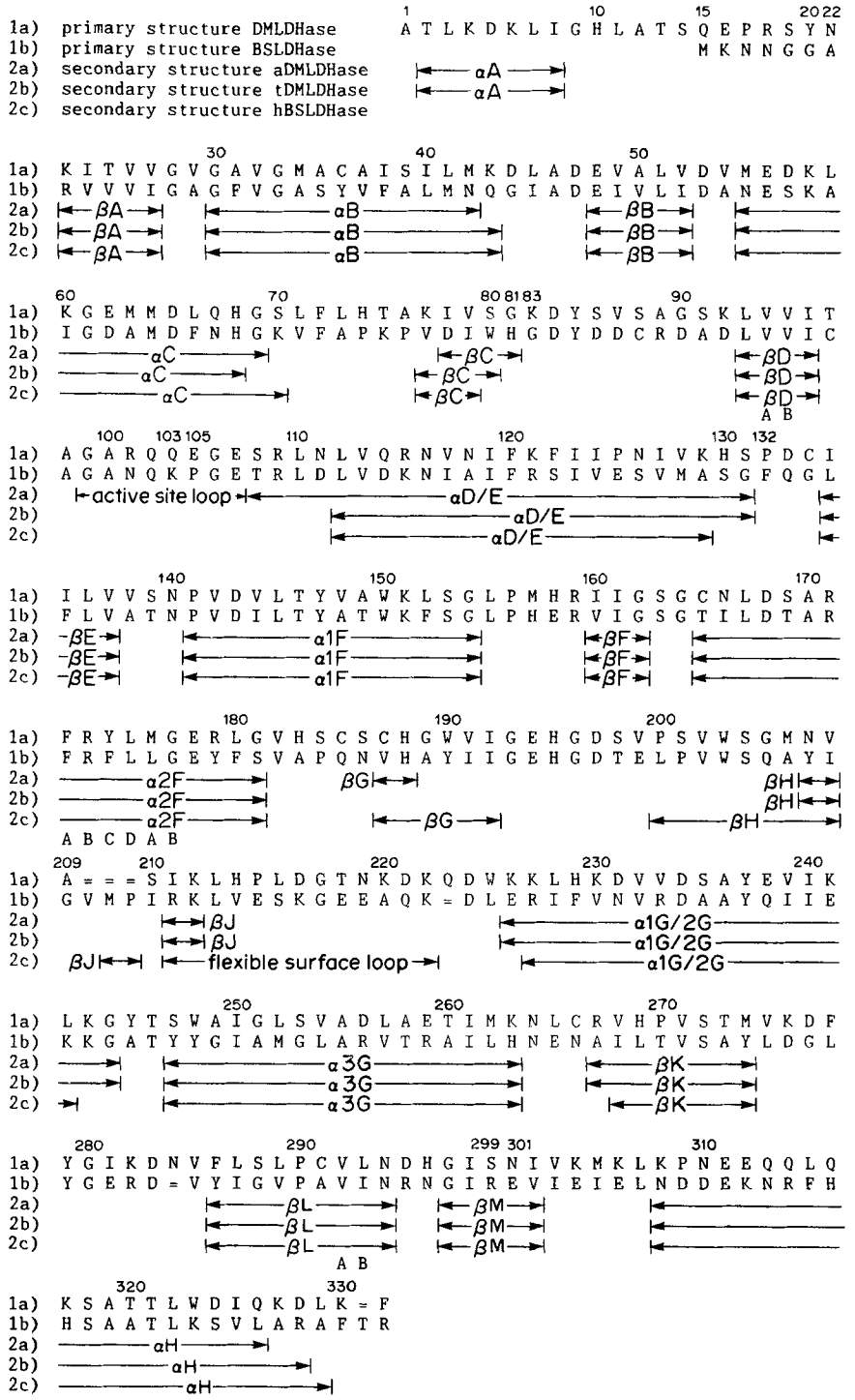

Fig. 2. Amino acid sequence of DMLDHase and BSLDHase and the assignment of the secondary structural elements to the aDMLDHase, tDMLDHase, and hBSLDHase structures. Residues are numbered according to Eventoff et al.[27] This numbering system is usually employed in the LDHase literature. It was used throughout this paper.

35 mA, using a Nonius oscillation camera.[30] The crystals were rotated about the c*-axis. Each film pack contained three films. Usually three exposures were made on one crystal before significant crystal damage was detected. Each individual photograph was oscillated through 2° with 0.4° overlap on adjacent films, covering a total of 60°. The films were digitized on an Optronics P1000 rotating drum film

TABLE I. Data Collection and Processing of "apo"- and holo-BSLDHase

	"apo"	holo
No. of photographs	38	36
Resolution (Å)	30.0–2.8	50.0–3.0
No. of measurements	128,751	76,407
No. of unique reflections	33,637	24,793
% of the theoretically possible no. of reflections	90.6	79.8
Scaling R-factor* (%)	9.1 [$I \geq 1.5\sigma(I)$]	10.9 [$I \geq 2.0\sigma(I)$]

The R-factor for scaling the two data sets together was 14.3%.

$$*R = \frac{\sum_h \sum_i |(I_h - I_{hi})|}{\sum_h \sum_i I_{hi}} \times 100$$

where I_h is the mean of the I_{hi} observations of reflection h.

scanner, using a 50 μm raster step. The data were processed, scaled together, and post-refined (Table I).[31,32]

Molecular Orientation and Position

Rotation functions[33] were used to determine the orientation of the molecular twofold axes[34] in the crystal unit cell. A self-rotation function (Fig. 3) was calculated using 376 large terms in the 11–6 Å resolution range. The coefficients were modified to remove the Patterson origin. The integration radius was 40 Å. An interpolation over the 27 nearest reciprocal lattice points was used for each non-integral lattice point. The rotation function was sampled in 3° intervals in ψ and φ, while κ was held constant at 180° (for definition of the spherical coordinates see Rossmann and Blow[33]).

The major peaks (A–E) on the low resolution rotation function are shown in Figure 3 and given in Table II. Due to the product of the crystallographic sixfold symmetry and any presumed twofold rotation orthogonal to the sixfold axis, there is a 12-fold rotation in the equator of the κ = 180° rotation function plane. Since the major peaks, other than the origin peak of the rotation function, are on the equator, peak B generates peak C and peak D generates peak E.

Two obvious solutions to the placement of the BSLDHase tetramer could be recognized on inspection of the rotation function. The first interpretation uses the larger peaks B and C in conjunction with peak A (which would then represent not only the crystallographic sixfold axis but also a parallel molecular twofold axis). The peaks A–C, or their symmetry-related positions, constitute an orthogonal set (Fig. 4). The second solution uses the lesser peaks D and E in a similar manner, but neglects the occurrence of the larger peaks B and C.

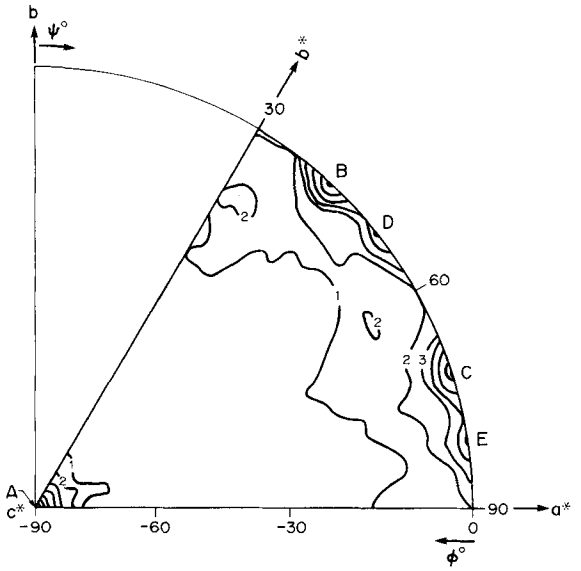

Fig. 3. Self-rotation function, using 11–6 Å resolution data. Peaks which were considered in the interpretation are labeled A–E (see Table II).

If there were a molecular twofold axis parallel to the crystallographic hexad, then there would be a very large peak in the Harker section (w = ½), whose coordinates would determine the position of the molecular center. Such a peak existed in a Patterson map, whose resolution was 12 Å or less, at u = 1, v = 1, w = ½. Introduction of higher resolution data rapidly eliminated this peak, suggesting that the molecular dyad was only roughly parallel to the c-axis. An alternative solution of the Patterson function would be u = v = 0, but that would cause 6 molecules to be stacked on top of each other along the 6_1 axis. Since c ≃ 360 Å, this solution would require a maximum molecular diameter of 60 Å, while the

TABLE II. Major Peaks in the Low Resolution (6 Å) Self-Rotation Function

Peak	Height	ψ (°)	ϕ (°)	κ (°)
A (origin)	100	90	−90	180
B	44	42	0	180
C	44	72	0	180
D	33	51	0	180
E	33	81	0	180

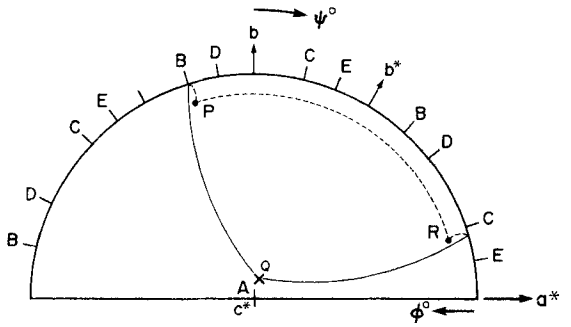

Fig. 4. Possible interpretation of the self-rotation function using the larger equatorial peaks B and C in conjunction with the origin peak A to orient the molecular twofold axes. The molecular axes are labeled in accordance with their later identification. However, note that the large peaks B, A, and C do not correspond precisely with the final molecular axes *P*, *Q*, and *R*, respectively.

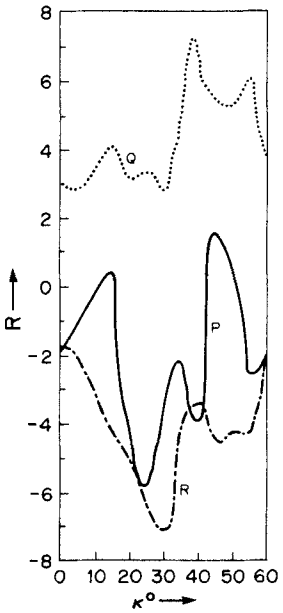

Fig. 5. Cross-rotation functions obtained by superimposing the molecular *P*-, *Q*-, and *R*-axes onto the crystallographic c* direction corresponding to peak A in the self-rotation function. The function explores relative rotations (κ) of the superimposed axes. There is a repetition after 60° on account of the crystallographic sixfold symmetry. The correct *Q*-axis superposition fits every 60° and, hence, also causes enhancement of the intermediate background.

known minimum diameter of LDHase is 72 Å. Thus the solution of u = v = 1, which places the molecule on a crystallographic 2_1 axis, was far more likely.

Cross-rotation functions (11–6 Å resolution) were calculated between aBSLDHase and aDMLDHase. Structure factors were calculated for a tetramer of aDMLDHase placed into a unit cell with its molecular *P*-, *Q*-, and *R*-axes[34] oriented along the *a*, *b*, and *c* cell edges, respectively, of a *P*222 cell with $a = b = c = 160$ Å, $\alpha = \beta = \gamma = 90°$. These large cell dimensions were chosen to avoid overlap of the self-Pattersons. The coordinates used for the F_c calculations were those of the polypeptide chain deposited with the Brookhaven Protein Data Bank for aDMLDHase, excluding the first 14 amino acids. The *P*-, *Q*-, and *R*-axes of the known structure were superimposed in turn on the directions corresponding to the peaks A–E in the self-rotation function of the unknown structure. The quality of each superposition was tested for all possible rotations about the aligned axes in 5° intervals (Fig. 5). The best results were obtained by placing the molecular *P*-, *Q*-, and *R*-axes close to the directions B, A, and C, respectively, in the self-rotation function (Fig. 4).

The Patterson function had shown that the molecular dyads are not precisely in the equatorial plane, nor parallel to the crystallographic *c*-axis, although the 6 Å resolution function was unable to resolve these orientations. Thus, a self-rotation function with 8–4 Å resolution data and a grid interval of 0.4° was calculated in the range ψ = 80° to 90° and ϕ = −90° to −80°. These calculations resulted in a local maximum at ψ = 84.6°, ϕ = −86.6°. Cross-rotation functions in which the molecular *Q*-axis was superimposed onto this self-rotation function direction gave improved orientations for the *P*- and *R*-axes. An exploration of the 4 Å resolution self-rotation function in the vicinity of the predicted orientation for the *P*- and *R*-axes also resulted in local maxima. These peaks were explored further with cross-rotation functions and were consistent within 0.4°. The final results from the rotation function studies are shown in Table IIIA.

A two-dimensional *R*-factor search was used to find a more precise molecular position (the *z* coordinate of the molecular center is arbitrary in the space group $P6_1$). A systematic *R*-factor search was made in the range x = 0.4 to 0.6, y = 0.4 to 0.6. The molecule was oriented in the same way in each of the positions six symmetry-related, first in space group $P6_1$ and then in space group $P6_5$. The *R*-factor was calculated for data between 10 and 6 Å resolution. The minimum *R*-factor was 47.7% at x = 0.460, y = 0.563 for the space group $P6_1$ (Fig. 6). For the five symmetry-related positions in $P6_1$, the *R*-factor ranged from 52.9 to 54.2% and for the six positions in $P6_5$ from 52.1 to 55.3%. Thus, the space group was established as $P6_1$ with respect to the

TABLE III. Molecular Orientation and Position

	Resolution of data (Å)	P ψ (°)	P φ (°)	Q ψ (°)	Q φ (°)	R ψ (°)	R φ (°)
A. Molecular orientation in the crystal cell							
"apo"-enzyme							
Cross-rotation function search	8–4	16.30	164.50	84.60	−86.60	74.67	4.88
R-factor search using aDMLDHase	11–6	17.20	157.23	82.64	−88.10	74.55	3.94
R-factor search using semi-refined BSLDHase	4.0–3.5	17.26	157.98	82.80	−88.04	74.40	3.99
holo-enzyme							
R-factor search using final refined "apo" coordinates	4.5–4.2	17.37	158.16	82.85	−88.21	74.26	3.82

	Resolution of data (Å)	Fractional coordinates x	y	z
B. Position of molecular center in the crystal cell				
"apo"-enzyme				
R-factor search using aDMLDHase	11–6	0.461	0.562	0.5000
R-factor search using semi-refined BSLDHase	4.0–3.5	0.4610	0.5613	0.5000
holo-enzyme				
R-factor search using final refined "apo" coordinates	4.5–4.2	0.4619	0.5627	0.5000

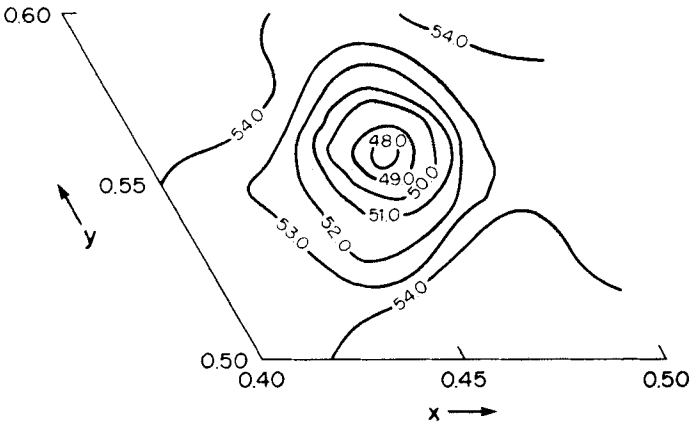

Fig. 6. Exploration of molecular position in terms of an *R*-factor. The minimum *R*-factor was 47.7% at x = 0.460, y = 0.563.

known hand of the BSLDHase molecule. (An alternative approach would have been to test the six possible molecular orientations at one selected molecular position for each of the two possible space groups.) A five-dimensional refinement of the position and orientation converged at $R = 45.9\%$ for 10–6 Å resolution data. The same parameters produced an *R*-factor of 48.6% for 15–3 Å resolution data.

Phase Improvement by Molecular Replacement

An approximate set of phases was now available based on the known aDMLDHase structure and the determination of the molecular orientation and position in the crystal cell. These phases were further iteratively refined using real-space averaging of the four noncrystallographic asymmetric units, with back-transformation of the averaged map.[35,36] This

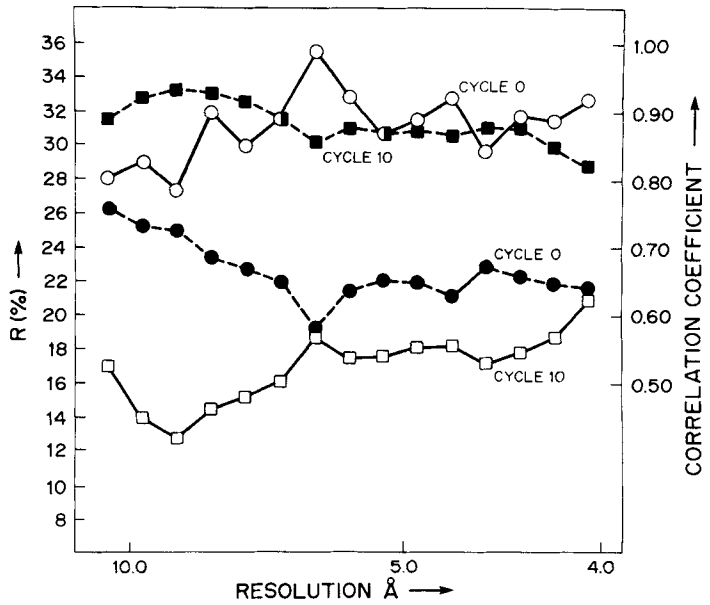

Fig. 7. After ten cycles of molecular replacement real-space averaging at 4.0 Å resolution, the *R*-factor had decreased to 17.3% and the correlation coefficient had increased to 0.88. Open circles (prior to refinement) or squares (after refinement) are *R*-factors. Black circles and squares are correlation coefficients, respectively. The *R*'-factor and correlation coefficient measure the agreement between observed amplitudes and amplitudes calculated by back-transformation of the averaged electron density in the crystal cell.

molecular replacement procedure requires knowledge of the molecular envelope in order to replace the averaged density in the crystal unit cell and to permit flattening of the density outside the molecular boundary. Although the tertiary structure of LDHase is well known, the available programs had been developed for structure determinations of viruses[37] and, thus, permitted only spherical envelopes. Hence, a molecular radius of 32 Å was chosen to extend over only the molecule, excluding all solvent regions. This included about 60% of the protein volume. Averaging was then performed inside the spherical envelope and solvent flattening was applied outside the molecular boundary, while the density between the sphere and the molecular boundary was left unchanged. The mask for the molecular envelope was developed using Wang's method[38] based on an $F_c e^{-i\alpha_c}$ map using the aDMLDHase coordinates.

Calculation of the *R*-factor as a function of resolution showed that the phasing model based on aDMLDHase was not acceptable (*R* greater than 50%) beyond 4 Å resolution. After ten cycles of molecular replacement real-space averaging limited to 4 Å resolution,[36,39] the *R*-factor had decreased to 17.3% and the correlation coefficient had increased to 0.88 (Fig. 7). The phases from 4 to 3 Å resolution were then determined by gradually increasing the resolution in small steps. Each step extended resolution by less than the first positive loop of a spherical diffraction function for the molecular radius of 32 Å. This implied an increase of about 1 to 2 reciprocal lattice units along a* or b* and about 5 reciprocal lattice units along c*. Eight to 10 cycles were performed until the procedure had essentially converged at each resolution step. The procedure was terminated (after a total of 61 cycles) at 3 Å resolution, where the sparsity of data suggested that there might be problems in further phase extension. The final *R*-factor was 13.8%, and the correlation coefficient was 0.92 (Fig. 8) for the aBSLDHase data (Table I). An averaged electron density map, skewed to place the molecular *P*-, *Q*-, and *R*-axes parallel to the sampling grid, was calculated based on the phases from the real-space averaging procedure with 15–3 Å resolution data.

Model Building and Refinement

A partial atomic model, based on the known amino acid sequence, was built into the aBSLDHase electron density with the use of an Evans and Sutherland PS300 computer graphics system and the FRODO program.[40,41] Major portions of the electron density map, particularly those parts in the sphere within which the density was averaged, could be readily interpreted. There was no apparent bias obtained from the initial 4 Å resolution phasing model that had been derived from the aDMLDHase structure. For instance, residue 278 was a Leu in BSLDHase but had been a Phe in the DMLDHase starting model. Although Leu 278 occurred outside the 32 Å sphere inside which the density had been

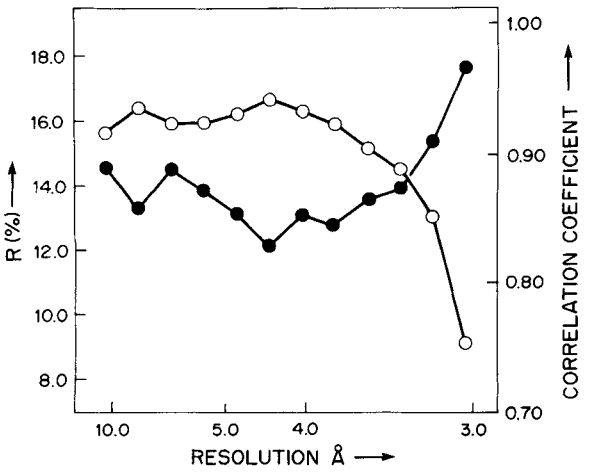

Fig. 8. Distribution of *R*-factors (black circles) and correlation coefficients (open circles) with resolution on completion of phase refinement using molecular replacement real-space averaging of electron density. After 61 cycles, the final overall *R*-factor was 13.8% and the overall correlation coefficient was 0.92. The rapid increase in the *R*-factor or decrease in the correlation coefficient in the highest resolution shell is due to the edge effect produced by exclusion of data beyond the resolution limit. During phase extension this edge effect is pushed to higher and higher resolution as the latter is gradually increased.

averaged, nevertheless there was no doubt about the identity of this residue. The first atomic model, built into a skewed and averaged electron density map, contained 1,961, out of a possible 2,459, non-hydrogen atoms of the polypeptide chain. This model gave an *R*-factor of 44% for data in the 15–3 Å resolution shell.

The restrained least-squares refinement program PROLSQ[42,43] was used for the refinement of the structure. The program, implemented on the Cyber 205 computer system at Purdue University, was modified with a vectorized subroutine for the calculation of structure factors and their derivatives.[44,45] The molecular 222 symmetry was imposed on the molecule by treating the noncrystallographic symmetry operators as constraints, thus reducing the refineable parameters to those in one molecular subunit. A full cycle of least-squares refinement, using about 2,500 atoms and 30,000 reflections between 6 and 2.8 Å resolution, required about 900 CPU seconds.

The course of the refinement for the "apo"-structure is shown in Table IV. The degree of restraint to idealized geometry is indicated by the r.m.s. deviation from ideal bond lengths. The final model included two sulfate ions per molecular subunit, corresponding to the substrate binding site and to the *P*-axis anion binding site, as was also found in aDMLDHase.[3] It excluded 23 residues which were not visible in an averaged ($2F_o - F_c$) electron density map. These residues were in the active site flexible loop (residues 102–110), in a mobile surface loop connecting βJ and αlG (residues 210B–222), and two amino acids (81 and 83) in a turn of the NADH binding domain (Fig. 2).

A long stretch of significant electron density was found in a position corresponding to the known NADH binding site in vertebrate LDHases. A model of the coenzyme, derived from tDMLDHase, fitted this density well. Comparison of the height of the density at the pyrophosphate moiety with that of the sulfates, when these ions were excluded from the structure factor calculations, gave an estimated occupancy of about 30–40% for the coenzyme. The most likely source of coenzyme was from the oxamate-Sepharose column used in purification which contained 0.2 mM NADH.[8] Yet optical absorption measurements at 260, 280, and 340 nm indicated that there was no significant amount of coenzyme bound to the enzyme. Apparently the dialysis steps, applied in later stages of purification, were not sufficient to remove the coenzyme completely (K_d = 1.5 μM).[23] As the partial occupancy of the coenzyme (possibly NADH, or perhaps an oxidized form of the coenzyme spectroscopically undetectable) may have caused conformational changes in some but not all of the subunits, further refinement was deemed suspect. Instead, refinement was continued on the completely substituted isomorphous holo-enzyme which had been crystallized in the presence of FBP.

The initial model of the holo-enzyme was the previously refined apo-enzyme structure, leaving out the two sulfate molecules and two residues within the flexible loop. As a first step in the refinement of the holo-enzyme, the orientation and position of the molecular *P*, *Q*, and *R*-symmetry axes were redetermined by using an *R*-factor minimization search. This resulted in only a 0.2° change of orientation (Table IIIA) and 0.04 Å shift of the molecular center (Table IIIB). The *R*-factor was then 30.4% for 4.5–4.2 Å resolution data (step 12 in Table IV).

Refinement then proceeded by means of a restrained least-squares approach, while maintaining the exact molecular 222 symmetry. The NADH coenzyme and FBP activator appeared as prominent features in the electron density map (Figs. 9, 10). The whole of NADH and one phosphate (representing a part of the activator molecule FBP) were included in the model of each subunit (step 15, Table IV). The complete FBP molecule was built into its electron density across the *P*-axis at the anion binding site in step 21 (Table IV). Another piece of high density was interpreted as a sulfate ion and also included in the model in step 21. This new anion binding site is close to the *R*-axis interface and the anion is hydrogen bonded to both subunits. No such ion has been found in the "apo" structure or any other LDHase.

Further cycles of least-squares refinement produced a final *R*-factor of 26.0%. The final model also included 50 water molecules. Omitted were residues

TABLE IV. Progress of Refinement

Compound	Operation	Resolution (Å)	Data selection	No. of reflections	No. of cycles	R(%) (at end)	B(Å^2)	No. of residues included out of 317	No. of atoms	r.m.s. deviation (Å) from idealized bond lengths at end of each refinement pass	Solvent included
"apo"	1. Least-squares refinement	10.0–3.0	$\mathbf{F} > 2\sigma(\mathbf{F})$	27,857	8	35.6	8.0	255	1,961	0.021	—
	2. Model rebuilt in graphics to a $(2\mathbf{F}_o - \mathbf{F}_c)$ electron density map										
	3. Least-squares refinement	10.0–3.0	$\mathbf{F} > 2\sigma(\mathbf{F})$	27,857	8	33.5	9.7	296	2,265	0.029	—
	4. Orientation and position of molecule was refined by an R-factor search with respect to current model (see Table III)										
	5. Model rebuilt with respect to a $(2\mathbf{F}_o - \mathbf{F}_c)$ electron density map										
	6.	8.0–3.0	$\mathbf{F} > 2\sigma(\mathbf{F})$	27,085	8	31.7	11.3	289	2,222	0.029	$2SO_4^{2-}$
	7.	6.0–2.8	$\mathbf{F} > 2\sigma(\mathbf{F})$	29,902	5	30.3	Indiv.	289	2,222	0.028	$2SO_4^{2-}$
	8. Model rebuilt with respect to a $(2\mathbf{F}_o - \mathbf{F}_c)$ electron density map										
	9.	6.0–2.8	$\mathbf{F} > 2\sigma(\mathbf{F})$	29,902	8	29.0	Indiv.	294	2,278	0.032	$2SO_4^{2-}$
	10. Model rebuilt with respect to a $(2\mathbf{F}_o - \mathbf{F}_c)$ electron density map										
	11.	6.0–2.8	$\mathbf{F} > 2\sigma(\mathbf{F})$	29,898	9	28.6	Indiv.	294	2,278	0.029	$2SO_4^{2-}$
holo	12. Orientation and position of the molecule was refined by an R-factor search with respect to the "apo" model (see Table III)										
	13	8.0–3.0	$\mathbf{F} > 2\sigma(\mathbf{F})$	23,184	0	30.3	Indiv.	292	2,261	0.029	—
	14. Least-squares refinement	8.0–3.0	$\mathbf{F} > 2\sigma(\mathbf{F})$	23,184	10	28.9	Indiv. ($\overline{B} = 16.7$)	292	2261	0.019	—
	15. Model rebuilt with respect to a $(\mathbf{F}_o - \mathbf{F}_c)$ electron density map										
	16. Least-squares refinement	6.0–3.0	$\mathbf{F} > 2\sigma(\mathbf{F})$	21,007	6	27.4	Indiv. ($\overline{B} = 16.2$)	298	2,363	0.022	$1SO_4^{2-}$ $1PO_4^{3-}$ 1NADH
	17. Model rebuilt with respect to $(n\mathbf{F}_o - \mathbf{F}_c)$* electron density maps, H_2O included										
	18. Least-squares refinement	6.0–3.0	$\mathbf{F} > 2\sigma(\mathbf{F})$	21,007	5	26.8	Indiv. ($\overline{B} = 16.1$)	301	2,425	0.023	$1SO_4^{2-}$ $1PO_4^{3-}$ 1NADH $35H_2O$
	19. Model rebuilt with respect to $(n\mathbf{F}_o - \mathbf{F}_c)$* electron density maps, H_2O included										
	20. Least-squares refinement	6.0–3.0	$\mathbf{F} > 2\sigma(\mathbf{F})$	21,007	3	26.4	Indiv. ($\overline{B} = 16.2$)	301	2,441	0.022	$1SO_4^{2-}$ $1PO_4^{3-}$ 1NADH $51H_2O$
	21. Model rebuilt with respect to $(n\mathbf{F}_o - \mathbf{F}_c)$* electron density maps										
	22. Least-squares refinement	6.0–3.0	$\mathbf{F} > 2\sigma(\mathbf{F})$	21,007	4	26.0	Indiv. ($\overline{B} = 15.7$)	301	2,460	0.019	$2SO_4^{2-}$ 1FBP 1NADH $50H_2O$

*n = 1,2.

101–109 from the active site flexible loop, residues 217–222 in a mobile surface loop (between βJ and α1G), and residues 81 and 83 (βC to βD) in a turn of the coenzyme binding domain. An unaveraged electron density map was calculated in order to determine whether the uninterpretable regions were due to disorder or due to a breakdown in the molecular symmetry. This map was based on phases computed from a model in which the difficult portions, plus segments leading to these residues, had been omit-

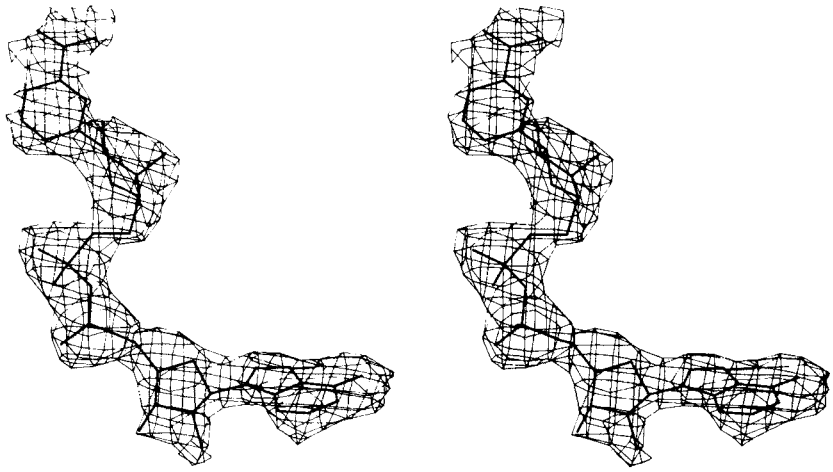

Fig. 9. Stereoscopic view showing the NADH molecule in its final ($2F_o - F_c$) electron density map for hBSLDHase.

ted. There were some areas (e.g., helix αD and residues 212–216) which had different conformations in the four individual subunits. Packing calculations showed that these portions of the structure are at intermolecular contact areas. A few cycles of refinement with four independent subunits lowered the *R*-factor to 23.2%, while no significant change of the molecular symmetry was observed (overall r.m.s. deviation of atomic position between the four subunits for all atoms was 0.11 Å and there were no regions where there were significantly larger deviations). Some side chains, especially surface arginines, showed different conformations within the four subunits. As the unaveraged map contained more noise than the averaged one and as the time required for inspecting about 1,300 residues was very large, further refinement was deemed too tedious in relation to the anticipated gain of information. Hence, the final model which was accepted and which is discussed here is that derived from the averaged map (step 22, Table IV). An example of the quality of the final averaged electron density map is given in Figure 11. The r.m.s. deviations from the ideal geometry for this final model are presented in Table V. These values are mostly in the range recommended by Hendrickson[46] and compare well with other refined protein structures of this size,[3,5,47] although the resolution was poorer and the data less complete for BSLDHase than for these other determinations. The final coordinates of the hBSLDHase model have been deposited with the Brookhaven Protein Data Bank.

RESULTS AND DISCUSSION

Conformation of Main Chain Angles

A Ramachandran plot[48] of the main chain dihedral angles φ and ψ (Fig. 12) shows 28 residues with positive φ angles, of which 14 belong to glycine residues (there are a total of 28 glycine residues in the subunit). The electron density corresponding to these glycine residues is of good quality. Nine of the 14 glycines with positive φ angles are conserved in all known LDHase sequences[9,27,49,50] and another four are conserved in all known bacterial LDHase sequences (Table VI).[9,51] Eight of the nine completely conserved glycine residues with positive φ angles in hBSLDHase also have positive φ angles in aDMLDHase[3] and tDMLDHase[6] (J. P. Griffith and M. G. Rossmann, unpublished results).* The ninth residue of this kind, Gly 99, is the "hinge" at the beginning of the active site flexible loop and does have a positive φ angle in the tDMLDHase structure. The positive φ value for Gly 99 may thus be necessary for the flexible loop to be in a closed conformation. All the glycine residues with positive φ angles are located in turns in the polypeptide chain and are often in the vicinity of functionally important amino acids. For example: i) Gly 193 and Gly 196 flank the essential His 195; ii) the carbonyl oxygen atom of Gly 44 (the equivalent residue in aDMLDHase, Asp 44, also has a positive φ angle) is hydrogen bonded to one oxygen atom of the sulfate near the *R*-axis interface; and iii) the carbonyl oxygen atom of Gly 209A is within hydrogen bonding distance to the side chain atom $N_{\epsilon 2}$ of His 188, which in turn is hydrogen bonded to the phosphate moiety of the FBP activator. There are 14 non-glycine residues with positive φ angles. Nine of these residues are in poorly ordered parts, especially Glu 214, Ser 215, Asp 224 between βH and α1G, and Phe 330A and Thr 330B in the C-terminus of the polypeptide chain. The remaining

*In tDMLDHase, the enzyme was co-crystallized with the coenzyme NADH and the substrate analogue oxamate.

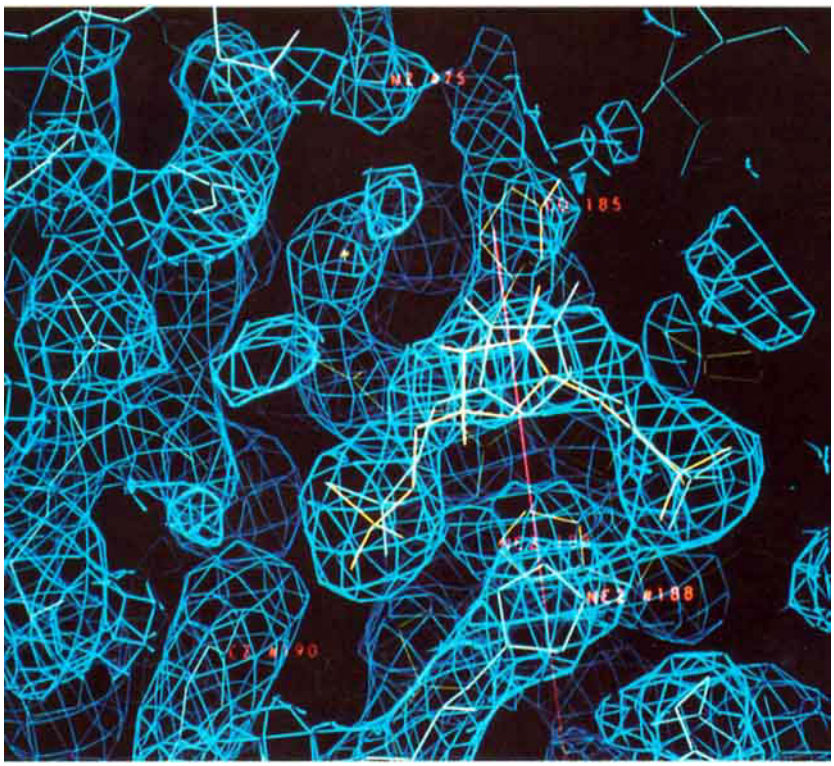

Figure 10. Legend appears on page 85.

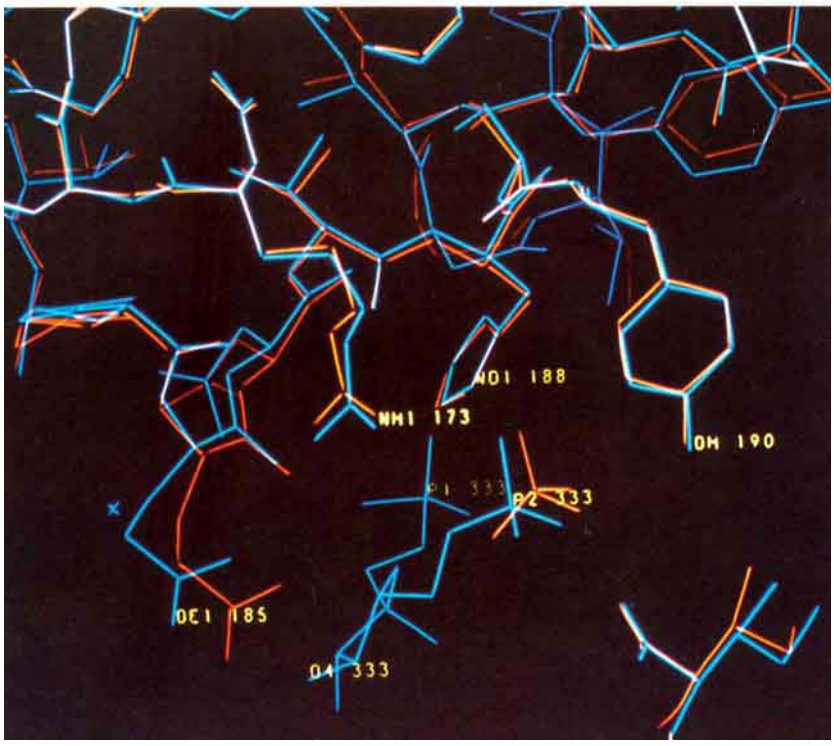

Figure 16. Legend appears on page 85.

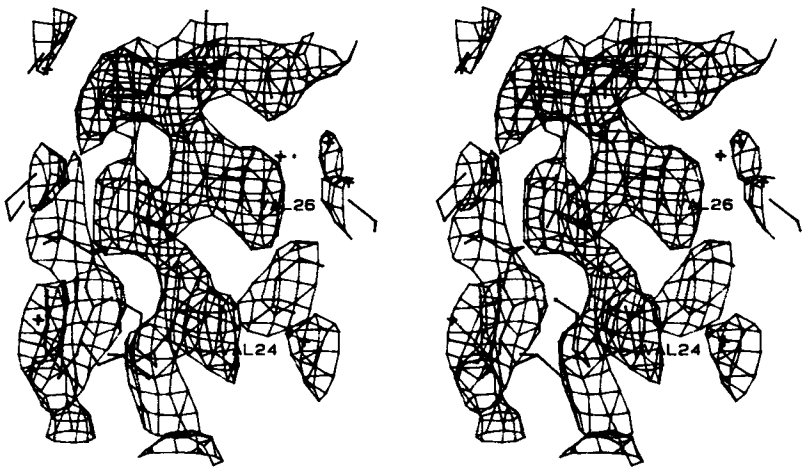

Fig. 11. Stereoscopic representation of part of βA in its final electron density map for hBSLDHase.

TABLE V. Deviations From Ideal Geometry for the Final Model of hBSLDHase

	r.m.s. deviation	
	Final value	Target value
Distances (Å)		
Bonds (1-2 neighbor)	0.019	(0.02)
Angles (1-3 neighbor)	0.043	(0.04)
Interplanar (1-4 neighbor)	0.046	(0.05)
Planar groups (Å)	0.023	(0.03)
Chiral centers (Å^3)	0.166	(0.17)
Torsion angles (°)		
Planar (0, 180)	5.8	(4.0)
Staggered (± 60, 180)	20.2	(15.0)
Orthonormal (± 90)	31.1	(20.0)
Non-bonded contacts (Å)		
Single torsion	0.249	(0.5)
Multiple torsion	0.304	(0.5)
Possible H-bond	0.254	(0.5)
Thermal factors (Å^2)		
Main-chain bond (1-2 neighbor)	0.96	(1.5)
Main-chain angle (1-3 neighbor)	1.72	(2.0)
Side-chain bond	1.36	(2.0)
Side-chain angle	2.32	(3.0)

five residues (Ala 245, Asn 264, Asn 266, Tyr 279, and Asn 294) are mostly conserved in bacterial LDHases and to a lesser extent in all known LDHase sequences. Among these, there are two residues (245 and 279) which also have positive ϕ angles in the two DMLDHase structures.

All but one of the ω main chain conformational angles (the torsion angle about the peptide bond) were restrained to the trans (ω = 180°) form in the refinement of the hBSLDHase structure. The only exception was between Asp 140 and Pro 141 for which a *cis* configuration resulted in a better geometry and a better fit to the electron density. This proline was also found to be in a *cis* configuration in the apo- and ternary DMLDHase.

The quality of the holo-model was tested by comparison with a data base containing 34 well-refined protein structures. The program PEPFLIP (kindly given to us by Alwyn Jones) takes sets of 5 residues of the hBSLDHase model at a time and searches for the 20 best fits to the C_α atoms in the data base. It then computes the distance between the carbonyl oxygen atom of the third residue of hBSLDHase with each of the top 20 least-squares fitted fragments from the data base. An r.m.s. value of these distances greater than, say, 2.5 Å is an indication that the conformation of the central residue might be in error. In the model of hBSLDHase there were 12 such cases (Table VII). Of these, two are adjacent to residues that were not fitted into the electron density (residues 81 and 83). Another two residues (Ser 163 and His 195) are associated with binding the coenzyme's nicotinamide moiety. This unusual conformation may have been induced by binding of the coenzyme. One residue (Gly 209A) has a positive ϕ angle (see above). However, five residues (Table VII) were at locations where the main chain density was ambiguous. In these cases the data base would suggest that the peptide bond of the present model perhaps should be flipped, although the electron density was equivocal.

Fig. 10. Computer graphics model of a portion of the hBSLDHase structure in its electron density. Here the two statistically disordered FDP molecules and the neighboring protein atoms are shown. The atoms of the reference subunit are shown inyellow,the atoms of the *P*-axis (red line) related subunit in white. The alternative conformation of Gln 185 can be seen with its corresponding electron density, but was not fitted.

Fig. 16. The FBP binding site region of hBSLDHase (blue) superimposed onto the sulfate binding region of aBSLDHase (red). The white color appears where the superposition of the two molecules is optimal.

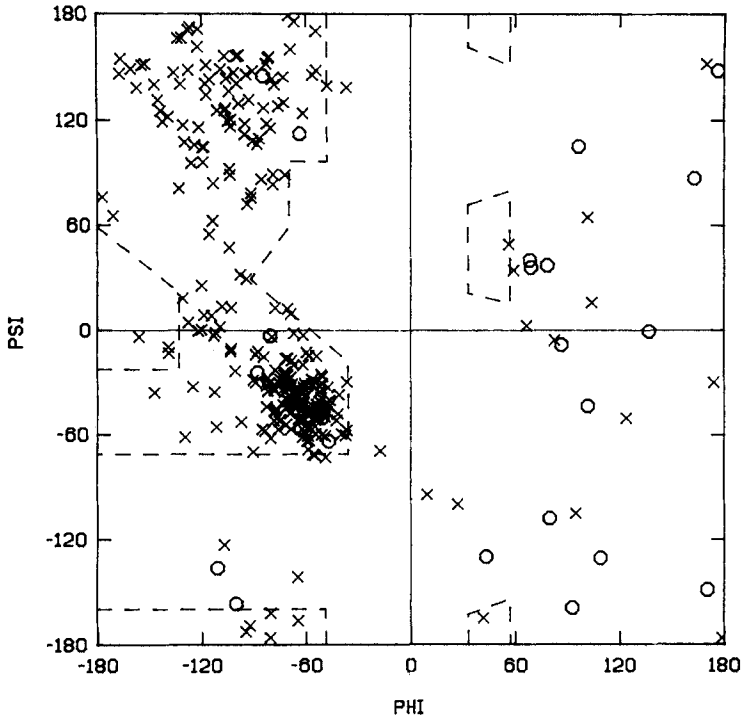

Fig. 12. Ramachandran plot of the main chain dihedral angles (ϕ, ψ) for hBSLDHase. The dashed lines enclose allowed regions for poly-L-alanine. Circles denote glycines.

TABLE VI. Comparison of Glycine Residues Associated With Positive ϕ Main Chain Angles in hBSLDHase With Respect to Their Equivalent Residues in Other Known LDHase Sequences*

Gly No.	Conserved in known LDHase sequences		Sign of ϕ angle	
	Vertebrates	Bacteria	aDMLDHase	tDMLDHase
19	Yes	No	−	−
28	Yes	Yes	+	+
44	No	Yes	+ (Asp)	+ (Asp)
99	Yes	Yes	−	+
131	No	Yes	−	−
154	Yes	Yes	+	+
164	Yes	Yes	+	+
193	Yes	Yes	+	+
196	Yes	Yes	+	+
209A	No	Yes	+ (Ala)	+ (Ala)
244	Yes	Yes	+	+
277	No	Yes	+ (Asp)	+ (Asp)
280	Yes	Yes	+	+
297	Yes	Yes	+	+

*The corresponding non-glycine residues are given in parentheses for the two DMLDHases.

The Fold of the Holo-Enzyme

Although binary complexes of LDHase with coenzyme have been studied,[52] there exist no high resolution refined structures of such binary complexes. Therefore, the hBSLDHase model was compared with the refined structures of aDMLDHase[3] (R =

TABLE VII. Residues in hBSLDHase That Have Suspect Main Chain Conformation Based on Deviation From Structures That Have Closely Matching Conformations in a Data Base of Well-Refined Protein Structures*

Residue	r.m.s. deviation of carbonyl oxygens from selected structures (Å)	Judgment		
		Probably wrong	Indeterminate	Probably correct
Ile 27	3.22			x
Pro 74	3.05		x	
Trp 80	2.65	x		
Asp 84	3.17	x		
Arg 89	2.51			x
Ser 163	2.53			x
His 195	2.85			x
Gly 209A	3.05			x
Glu 265	3.22		x	
Asp 276	2.63		x	
Arg 282	3.08		x	
Ala 329	3.05	x		

*These positions were re-inspected and judged for a likelihood of correctness based on appearance of the electron density map and local stereochemistry.

20.2% for 8 to 2 Å resolution data, r.m.s. deviation of bond length from ideal values was 0.026 Å) and of tDMLDHase[6] (R = 17.3% for 6 to 2.1 Å resolution data, r.m.s. deviation of bond length from ideal values was 0.018 Å; J. P. Griffith & M. G. Rossmann, unpublished results). The purpose was in part to determine whether the apo or ternary structure resembles the hBSLDHase structure more closely.

A program supplied to us by Dr. W. Kabsch[53] was used to assign systematically the secondary structural elements of all three LDHase structures (Fig. 2). The fold of the polypeptide chain of hBSLDHase is essentially the same as that of DMLDHase.[1] However, there are some significant differences among the three structures.

1. The first 14 residues are absent in hBSLDHase, thus the major part of the N-terminal arm is missing.
2. The kink which separates αD from αE, at a proline in DMLDHase, is not pronounced in hBSLDHase.
3. The flexible active site loop is mostly disordered (residues 101–109) in hBSLDHase.
4. Part of a flexible surface loop (between βH and α1G, residues 217–222) is disordered in hBSLDHase.
5. The antiparallel β-strand, βH, extends further (residues 200–206) in hBSLDHase than in either DMLDHase structure.
6. Helix αH is one turn longer at the C-terminus in hBSLDHase and tDMLDHase than in aDMLDHase.
7. Helix αH is shifted and rotated in hBSLDHase and tDMLDHase with respect to the aDMLDHase structure.

A systematic comparison of the overall fold of the three structures (hBSLDHase, aDMLDHase and tDMLDHase) was accomplished by comparing the C_α coordinates. The first comparison merely superimposed the common P, Q, R molecular axes. This shows the gross conformational changes in the tetramer. In the second comparison the coordinates of selected C_α atoms were superimposed by a least-squares method.[54,55] These comparisons were done pairwise for the whole subunit and for the equivalent individual secondary structural elements (Table VIII).

The largest difference occurs in helix αH. The helix of the apo structure is moved by 1.2 Å and 3.2 Å along the helix axis, and is rotated by 4.7° and 8.0°, relative to hBSLDHase and tDMLDHase, respectively. Conformational changes in the active center region are likely to communicate themselves to helix αH by an interaction of the turn between βG and βH, which contains the essential His 195, and the conserved Ser 318 in helix αH. While in the aDMLDHase structure there is only one hydrogen bond between the hydroxyl of Ser 318 in αH and the rest of the enzyme, in tDMLDHase there are two quite different hydrogen bonds because of the large shift in the position of helix αH. In aDMLDHase Ser 318 is hydrogen bonded to the carboxy group of Glu 194 (Fig. 13a), in tDMLDHase Ser 318 is hydrogen bonded to the main chain nitrogen of residue 194 and the hydroxyl of Ser 198 (Fig. 13b). The same hydrogen bonding pattern as in tDMLDHase was also found in the hBSLDHase structure, where Ser 198 is replaced by a Thr (Fig. 13c). (The starting model for the hBSLDHase structure was aDMLDHase, *not* tDMLDHase. Furthermore, the whole of αH had been omitted in order to assign its correct position in hBSLDHase.) The side chain tor-

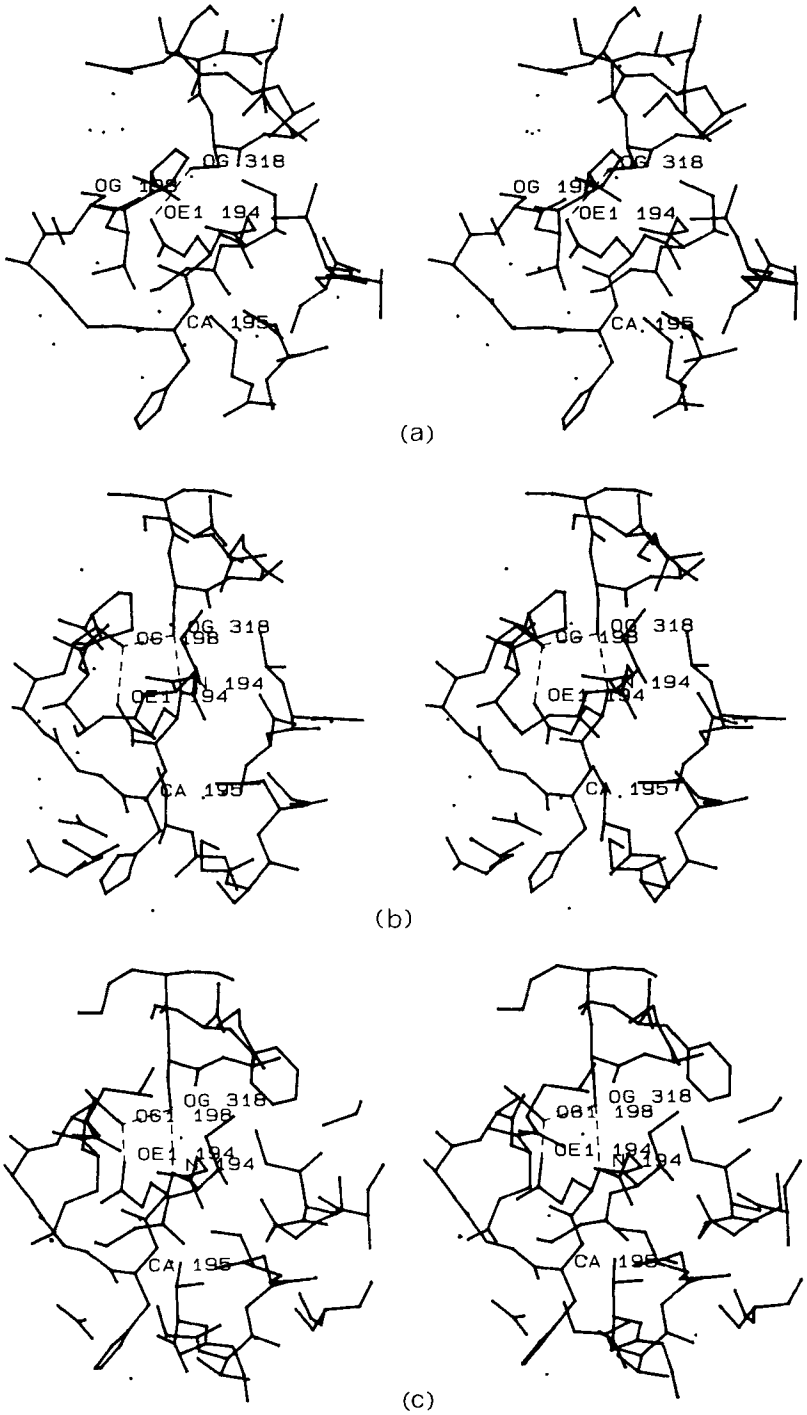

Fig. 13. Stereoscopic view of the conserved residue Ser 318 and its close environment in **a)** aDMLDHase, **b)** tDMLDHase, **c)** hBSLDHase.

sion angle of Ser 318 is in the *trans* range (χ_1 = 180°) for both coenzyme bound structures, but in the *–gauche* range (χ_1 = −60°) for the apo-enzyme structure. Similarly, the side chain torsion angle of residue 198 is in the *+gauche* range (χ_1 = 60°) for both coenzyme bound structures, but in the *−gauche* range (χ_1 = −60°) for the apo-enzyme. The conformation of the turn region between βG and βH in hBSLDHase has greater similarity to the ternary than to the apo DMLDHase structure. These obser-

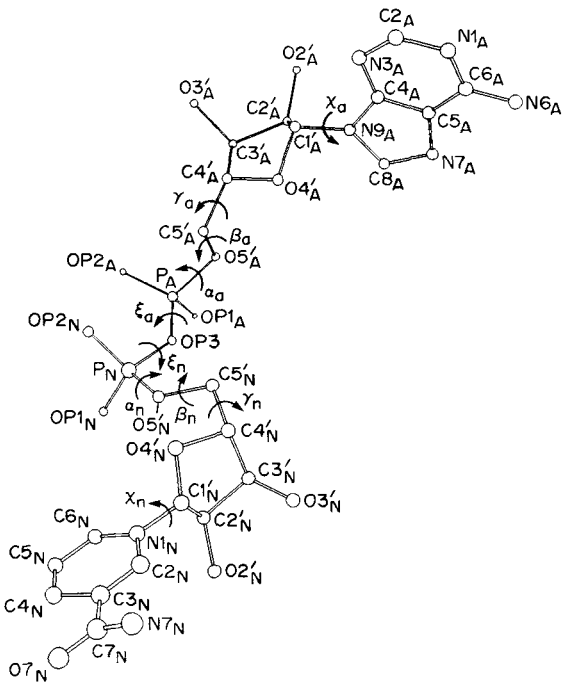

Fig. 14. Schematic representation of the molecule NADH with the names of the coenzyme atoms and torsion angles used in this paper.

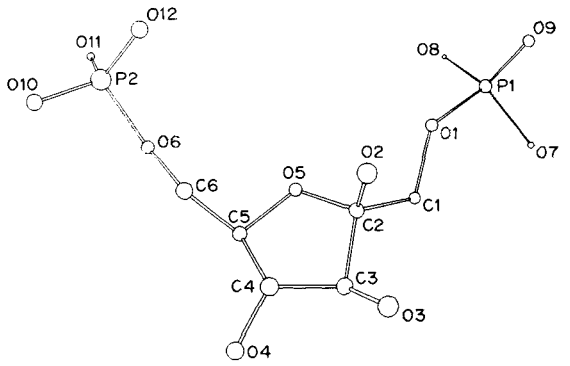

Fig. 15. Schematic drawing of the molecule FBP and the nomenclature of the atoms used here.

vations suggest that the binding of the coenzyme causes a shift of His 195 which triggers the movement of helix αH. Crystals of hBSLDHase shatter when soaked with oxamate, suggesting that the active site loop is not completely closed as observed in tDMLDHase. Thus, the loop displacement is not initialized by the movement of helix αH but rather by binding of substrate. This result is in agreement with those from experiments by Atkinson et al.,[56] who observed a loop movement by measuring the change in fluorescence of a tryptophan in a binary complex of a mutant (Gly 106 → Trp) when substrate was added. The position of the active site loop in apo and holo structures varies considerably.[5] This suggests that the loop in the apo- and holo-enzyme may have many different conformations, some of which are observed in the available crystal structures.

Another major change occurs in the somewhat disordered helices α1G and α2G, where a rotation of 8.3° and 5.7° takes place in the coenzyme-bound structures in comparison with the apo structure. Thus, binding of coenzyme causes similar conformational changes in both BSLDHase and DMLDHase. Other changes seen in Table VIII are correlated with species differences.

The NADH Site

The electron density corresponding to the coenzyme molecule NADH represents a very well defined feature of the hBSLDHase structure (Fig. 9). Its overall geometry and relative position in the enzyme is very similar to that found in tDMLDHase.

The best fit to the electron density was achieved when both ribose rings were considered to have ^2E (C2′-*endo*) puckering. Both the adenine and the nicotinamide ring are in an *anti* conformation and are roughly perpendicular to each other.

A parameter which is frequently used to measure the extension of the coenzyme[57] is the distance between C6 of the adenine and C2 of the nicotinamide ring (Fig. 14). This value is 15 Å for NADH bound to hBSLDHase, which is practically the same as for an NADH molecule bound to DMLDHase (14.9 Å) or to horse LADHase (15 Å).[58]

The torsion angles for the coenzyme, shown in Table IX, are very similar to those of the coenzyme in the tDMLDHase structure. However, there is some variation of these angles in other NADH and NAD^+ structures (for a more extensive comparison see Eklund et al.[58]). The angles for the AMP part are close to those in the small molecule structure of Li-NAD^+,[59] while the angles in the NMN part are close to those found in tLADHase.[58] The angles χ_a and χ_n of the coenzyme in hBSLDHase and tLADHase are close to −120°, consistent with an independent estimate based on a measurement of the proton-proton transferred nuclear Overhauser enhancement in NAD^+ bound to liver and yeast ADHase in solution.[60]

A sulfate ion occupies the substrate site in hBSLDHase, as in aDMLDHase.[3,61] This anion is essentially at the same position as the carboxylate group of the substrate analogue oxamate in the tDMLDHase complex. The carboxyamide of the nicotinamide moiety has approximately a 12° rotation

TABLE VIII. Comparison of a) hBSLDHase With aDMLDHase, b) hBSLDHase With tDMLDHase, and c) aDMLDHase With tDMLDHase

Structural element	Superposition of molecular axes* (Å)			Best superposition of C_α atoms† (Å)			Rotation‡ (°)			Shift along rotation axis (Å)		
	a	b	c	a	b	c	a	b	c	a	b	c
Subunit**	1.5	1.6	1.4	1.5	1.4	1.2	1.2	0.3	0.9	−0.02	0.14	−0.47
β-sheets												
Parallel sheet (strands A, B, C, D, E, F)	1.0	1.2	0.7	0.7	0.6	0.3	1.0	1.5	1.3	−0.33	−0.77	−0.71
Antiparallel sheet (strands G, H, J)	0.9	1.4	0.7	0.4	0.4	0.2	9.9	10.0	2.3	−0.13	0.09	0.52
Antiparallel sheet (strands K, L, M)	0.9	1.2	0.6	0.6	0.6	0.3	4.3	1.5	2.0	−0.94	0.59	−1.18
α-helices												
αB	0.9	1.4	0.8	0.3	0.4	0.3	5.8	8.1	2.6	1.2	1.44	0.39
αC	0.7	0.8	0.7	0.3	0.3	0.1	5.2	6.0	0.9	−0.14	−0.43	−0.64
αD/E	1.6	1.3	1.3	0.9	0.8	0.7	7.7	3.1	7.1	−1.19	−0.68	−2.73
α1F	0.6	0.8	0.8	0.3	0.3	0.2	4.3	3.7	7.0	1.59	−1.54	−0.32
α2F	0.7	1.0	0.6	0.4	0.4	0.3	5.0	6.6	1.8	−0.15	−0.18	0.06
α1G/2G	1.1	1.3	1.2	0.9	0.5	0.7	8.3	2.7	5.7	1.83	0.04	0.50
α3G	0.9	1.1	0.7	0.4	0.3	0.2	2.6	0.9	2.1	−0.33	−0.82	0.34
αH	2.5	1.0	2.4	0.6	0.5	0.4	4.7	3.0	8.0	−1.24	−0.28	−3.20

*Root-mean-square differences between C_α atoms on superposition of molecular *P*-, *Q*-, and *R*-axes.
†Root-mean-square differences between C_α atoms after least-squares superposition of the individual structural units of a single subunit.
‡Rotational component of least-squares superposition.
**Residues 1–14 of the two DMLDHases were excluded from the calculations.

out of the plane of the pyridine ring. This allows formation of a hydrogen bond between the N7N atom (Fig. 14) of the amide and the hydroxyl of Ser 163.

The FBP Site

The activator molecule FBP binds directly on the molecular *P*-axis such that the two phosphate moieties occupy twofold-symmetric anion binding sites across the *P*-axis (Fig. 10). Thus, there are two FBP molecules per tetrameric hBSLDHase, consistent with the results of Clarke et al.[19]

The conformation about the C1-C2 and C5-C6 bonds are *gauche-trans* (gt) in both cases (Fig. 15), if it is assumed that the furanose ring is in the ^3E (C3′-*endo*) conformation with respect to the C6 atom. This puckering was also found in the FBP molecule of the trisodium salt structure[62] where there is a gg and gt conformation for the C1-C2 and C5-C6 bond, respectively.

The molecular *P*-axis lies approximately in the fructose ring. As the FBP molecule is only a pseudo twofold symmetric molecule, it binds to the enzyme in two orientations which are related by the molecular twofold *P*-axis (Fig. 10). This results in alternative conformations of the protein environment in the vicinity of the FBP molecule. There are two possible conformations of the Gln 185 side chain in a $(2F_o - F_c)$ electron density map (Fig. 10). One of the conformations of Gln 185 is hydrogen bonded to the FBP molecules in one of its two possible orientations. The alternative Gln 185 conformation would cause steric hindrance with the same FBP molecule. A difference between eukaryotic and prokaryotic LDHases is that the latter require the binding of FBP as an activator. A comparison of the activator site in hBSLDHase with the corresponding anion binding sites in apo- and ternary DMLDHase[61] showed no significant differences in the residues which are involved in binding to the anions. The only noticeable difference between the hBSLDHase and aBSLDHase structures in the vicinity of the FBP binding site is at Gln 185. The side chain of this amino acid has moved about 1.5 Å away from the FBP molecule in hBSLDHase, allowing formation of hydrogen bonds to the furanose part of the activator molecule (Fig. 16). In contrast, in aBSLDHase Gln 185 can approach closer to the bound sulfate anion as there is no steric hindrance with a bound FBP molecule. However, what is not known is the structure of this site in the absence of either FBP or an anion. The site of phosphate binding in hBSLDHase differs slightly from the sulfate binding site in aBSLDHase. The sulfate anion is hydrogen bonded to Tyr 190; however, the phosphate moiety is about 0.7 Å further away and thus closer to His 188 and Arg 173. Hence, the phosphate would be a better neutralizer of charges on the histidine and arginine residues which themselves are close to the substrate

TABLE IX. Conformational Parameters of NADH Bound to BSLDHase, DMLDHase, Horse LADHase, and of the Small Molecule Structure Li-NAD$^+$

	χ_a	γ_a	β_a	α_a	ξ_a	ξ_n	α_n	β_n	γ_n	χ_n
BSLDHase	−133	34	−149	−64	133	−165	9	−162	87	−124
DMLDHase	−108	45	−138	−76	115	−148	63	−179	58	−106
LADHase	−96	−79	147	106	85	−153	59	−146	39	−102
Li-NAD$^+$	−121	48	163	−125	133	72	79	179	47	−165

binding residue Arg 171 on helix α2F. Therefore, a structure of hBSLDHase without an anion at the *P*-axis (FBP) binding site would be of particular interest.

ACKNOWLEDGMENTS

We are grateful to M. V. Hosur, Ignacio Fita, James P. Griffith, and S. Krishnaswamy for helpful discussions concerning the crystallographic techniques and to Greg Kamer for assistance in setting up the Wang masking program to determine the molecular envelope. We thank Sharon Fateley, Sharon Wilder, and Patricia Trobisch for help in the preparation of this manuscript. The work was supported by grants from the Eidgenössische Technische Hochschule to K.P., H.P.S., and H.Z. (Kredit für Unterricht und Forschung and Schweizerischer Nationalfonds) and a National Institutes of Health grant to M.G.R.

REFERENCES

1. Holbrook, J.J., Liljas, A., Steindel, S.J., Rossmann, M.G. Lactate dehydrogenase. In: "The Enzymes," 3rd edn., Vol. XI. Boyer, P.D. (ed.). New York: Academic Press, 1975: 191–292.
2. Adams, M.J., Ford, G.C., Koekoek, R., Lentz, P.J., Jr., McPherson, A., Jr., Rossmann, M.G., Smiley, I.E., Schevitz, R.W., Wonacott, A.J. Structure of lactate dehydrogenase at 2.8 Å resolution. Nature (Lond.) 227:1098–1103, 1970.
3. Abad-Zapatero, C., Griffith, J.P., Sussman, J.L., Rossmann, M.G. Refined crystal structure of dogfish M_4 apolactate dehydrogenase. J. Mol. Biol. 198:445–467, 1987.
4. Musick, W.D.L., Rossmann, M.G. The structure of mouse testicular lactate dehydrogenase isoenzyme C_4 at 2.9 Å resolution. J. Biol. Chem. 254:7611–7620, 1979.
5. Hogrefe, H.H., Griffith, J.P., Rossmann, M.G., Goldberg, E. Characterization of the antigenic sites on the refined 3-Å resolution structure of mouse testicular lactate dehydrogenase C_4. J. Biol. Chem. 262:13155–13162, 1987.
6. White, J.L., Hackert, M.L., Buehner, M., Adams, M.J., Ford, G.C., Lentz, P.J., Jr., Smiley, I.E., Steindel, S.J., Rossmann, M.G. A comparison of the structures of apo dogfish M_4 lactate dehydrogenase and its ternary complexes. J. Mol. Biol. 102:759–779, 1976.
7. Grau, U.M., Trommer, W.E., Rossmann, M.G. Structure of the active ternary complex of pig heart lactate dehydrogenase with *S*-lac-NAD$^+$ at 2.7 Å resolution. J. Mol. Biol. 151:289–307, 1981.
8. Schär, H.P., Zuber, H. Structure and function of L-lactate dehydrogenases from thermophilic and mesophilic bacteria. I) Isolation and characterization of lactate dehydrogenases from thermophilic and mesophilic bacilli. Hoppe Seylers Z. Physiol. Chem. 360:795–807, 1979.
9. Hensel, R., Mayr, U., Yang, C.Y. The complete primary structure of the allosteric L-lactate dehydrogenase from *Lactobacillus casei*. Eur. J. Biochem. 134:503–511, 1983.
10. Crossley, L.G., Jago, G.R., Davidson, B.E. Partial sequence data for the L-(+)-lactate dehydrogenase from *Streptococcus cremoris* US3 including the amino acid sequences around the single cysteine residue and at the N-terminus. Biochim. Biophys. Acta 581:342–355, 1979.
11. Adams, M.J., Buehner, M., Chandrasekhar, K., Ford, G.C., Hackert, M.L., Liljas, A., Lentz, P.J., Jr., Rao, S.T., Rossmann, M.G., Smiley, I.E., White, J.L. Subunit interactions in lactate dehydrogenase. In: "Protein-Protein Interactions." Jaenicke, R., Helmreich, E. (eds.). Berlin: Springer-Verlag, 1972:139–156.
12. Garvie, E.I. Bacterial lactate dehydrogenases. Microbiol. Rev. 44:106–139, 1980.
13. Kelly, N., Delaney, M., O'Carra, P. Affinity chromatography of bacterial lactate dehydrogenases. Biochem. J. 171: 543–547, 1978.
14. Crow, V.L., Pritchard, G.G. Fructose 1,6-diphosphate-activated L-lactate dehydrogenase from *Streptococcus lactis:* Kinetic properties and factors affecting activation. J. Bacteriol. 131:82–91, 1977.
15. Hensel, R., Mayr, U., Stetter, K.O., Kandler, O. Comparative studies of lactic acid dehydrogenases in lactic acid bacteria. I. Purification and kinetics of the allosteric L-lactic acid dehydrogenase from *Lactobacillus casei* ssp. *casei* and *Lactobacillus curvatus*. Arch. Microbiol. 112:81–93, 1977.
16. Amelunxen, R.E., Murdock, A.L. Mechanisms of thermophily. CRC Crit. Rev. Microbiol. 6:343–393, 1978.
17. Zuber, H. Comparative studies of thermophilic and mesophilic enzymes: Objectives, problems, results. In: "Biochemistry of Thermophily." Friedman, S.M. (ed.). New York: Academic Press, 1978:267–285.
18. Zuber, H. Temperature adaptation of lactate dehydrogenase. Structural, functional and genetic aspects. Biophys. Chem. 29:171–179, 1988.
19. Clarke, A.R., Evington, J.R.N., Dunn, C.R., Atkinson, T., Holbrook, J.J. The molecular pathway by which fructose 1,6-bisphosphate induces the assembly of a bacterial lactate dehydrogenase. Biochim. Biophys. Acta 870:112–126, 1986.
20. Wirz, B., Suter, F., Zuber, H. Structure and function of L-lactate dehydrogenases from thermophilic and mesophilic bacteria. III) The primary structure of thermophilic lactate dehydrogenase from *Bacillus stearothermophilus*. Hydroxylamine-, *o*-iodosobenzoic acid- and tryptic-fragments. The complete amino-acid sequence. Hoppe Seylers Z. Physiol. Chem. 364:893–909, 1983.
21. Barstow, D.A., Clarke, A.R., Chia, W.N., Wigley, D., Sharman, A.F., Holbrook, J.J., Atkinson, T., Minton, N.P. Cloning, expression and complete nucleotide sequence of the *Bacillus stearothermophilus* L-lactate dehydrogenase gene. Gene 46:47–55, 1986.
22. Zülli, F., Weber, H., Zuber, H. Structure and function of L-lactate dehydrogenases from thermophilic and mesophilic bacteria, VI. Nucleotide sequences of lactate dehydrogenase genes from the thermophilic bacteria *Bacillus stearothermophilus, B. caldolyticus* and *B. caldotenax*. Biol. Chem. Hoppe Seyler 368:1167–1177, 1987.
23. Clarke, A.R., Atkinson, T., Campbell, J.W., Holbrook, J.J. The assembly mechanism of the lactate dehydrogenase tetramer from *Bacillus stearothermophilus;* the equilibrium relationships between quaternary structure and the binding of fructose 1,6-bisphosphate, NADH and oxamate. Biochim. Biophys. Acta 829:387–396, 1985.
24. Clarke, A.R., Wigley, D.B., Chia, W.N., Barstow, D., Atkinson, T., Holbrook, J.J. Site-directed mutagenesis reveals role of mobile arginine residue in lactate dehydrogenase catalysis. Nature (Lond.) 324:699–702, 1986.
25. Clarke, A.R., Smith, C.J., Hart, K.W., Wilks, H.M., Chia, W.N., Lee, T.V., Birktoft, J.J., Banaszak, L.J., Barstow, D.A., Atkinson, T., Holbrook, J.J. Rational construction of

a 2-hydroxyacid dehydrogenase with new substrate specificity. Biochem. Biophys. Res. Commun. 148:15–23, 1987.
26. Waldvogel, S., Weber, H., Zuber, H. Structure and function of L-lactate dehydrogenases from thermophilic and mesophilic bacteria VII. Nucleotide sequence of the lactate dehydrogenase gene from the mesophilic bacterium *Bacillus megaterium*. Preparation and properties of a hybrid lactate dehydrogenase comprising moieties of the *B. megaterium* and *B. stearothermophilus* enzymes. Biol. Chem. Hoppe Seyler 368:1391–1399, 1987.
27. Eventoff, W., Rossmann, M.G., Taylor, S.S., Torff, H.J., Meyer, H., Keil, W., Kiltz, H.H. Structural adaptations of lactate dehydrogenase isozymes. Proc. Natl. Acad. Sci. USA 74:2677–2681, 1977.
28. Schär, H.P., Zuber, H., Rossmann, M.G. Crystallization of lactate dehydrogenase from *Bacillus stearothermophilus*. J. Mol. Biol. 154:349–353, 1982.
29. Matthews, B.W. Solvent content of protein crystals. J. Mol. Biol. 33:491–497, 1968.
30. Arndt, U.W., Wonacott, A.J. "The Rotation Method in Crystallography." Amsterdam: North-Holland, 1977.
31. Rossmann, M.G. Processing oscillation diffraction data for very large unit cells with an automatic convolution technique and profile fitting. J. Appl. Crystallogr. 12:225–238, 1979.
32. Rossmann, M.G., Leslie, A.G.W., Abdel-Meguid, S.S., Tsukihara, T. Processing and post-refinement of oscillation camera data. J. Appl. Crystallogr. 12:570–581, 1979.
33. Rossmann, M.G., Blow, D.M. The detection of sub-units within the crystallographic asymmetric unit. Acta Crystallogr. 15:24–31, 1962.
34. Rossmann, M.G., Adams, M.J., Buehner, M., Ford, G.C., Hackert, M.L., Liljas, A., Rao, S.T., Banaszak, L.J., Hill, E., Tsernoglou, D., Webb, L. Molecular symmetry axes and subunit interfaces in certain dehydrogenases. J. Mol. Biol. 76:533–537, 1973.
35. Bricogne, G. Methods and programs for direct space exploitation of geometric redundancies. Acta Crystallogr. A32:832–847, 1976.
36. Argos, P., Ford, G.C., Rossmann, M.G. An application of the molecular replacement technique in direct space to a known protein structure. Acta Crystallogr. A31:499–506, 1975.
37. Johnson, J.E. Appendix II. Averaging of electron density maps. Acta Crystallogr. B34:576–577, 1978.
38. Wang, B.C. Resolution of phase ambiguity in macromolecular crystallography. Methods Enzymol. 115:90–112, 1985.
39. Arnold, E., Vriend, G., Luo, M., Griffith, J.P., Kamer, G., Erickson, J.W., Johnson, J.E., Rossmann, M.G. The structure determination of a common cold virus, human rhinovirus 14. Acta Crystallogr. A43:346–361, 1987.
40. Jones, T.A. A graphics model building and refinement system for macromolecules. J. Appl. Crystallogr. 11:268–272, 1978.
41. Jones, T.A. Frodo: A graphics fitting program for macromolecules. In: "Computational Crystallography." Sayre, D. (ed.). Oxford: Clarendon Press, 1982:303–317.
42. Hendrickson, W.A., Konnert, J.H. Stereochemically restrained crystallographic least-squares refinement of macromolecule structures. In: "Biomolecular Structure, Conformation, Function, and Evolution," Vol. 1. Srinivasan, R. (ed.). Oxford: Pergamon Press, 1981:43–57.
43. Konnert, J.H. A restrained-parameter structure-factor least-squares refinement procedure for large asymmetric units. Acta Crystallogr. A32:614–617, 1976.
44. Fita, I., Silva, A.M., Murthy, M.R.N., Rossmann, M.G. The refined structure of beef liver catalase at 2.5 Å resolution. Acta Crystallogr. B42:497–515, 1986.
45. Silva, A.M., Rossmann, M.G. The refinement of southern bean mosaic virus in reciprocal space. Acta Crystallogr. B41:147–157, 1985.
46. Hendrickson, W.A. Stereochemically restrained refinement of macromolecular structures. Methods Enzymol. 115:252–270, 1985.
47. Skarżyński, T., Moody, P.C.E., Wonacott, A.J. Structure of holo-glyceraldehyde-3-phosphate dehydrogenase from *Bacillus stearothermophilus* at 1.8 Å resolution. J. Mol. Biol. 193:171–187, 1987.
48. Ramachandran, G.N., Ramakrishnan, C., Sasisekharan, V. Stereochemistry of polypeptide chain configurations. J. Mol. Biol. 7:95–99, 1963.
49. Li, S.S.L., Fitch, W.M., Pan, Y.C.E., Sharief, F.S. Evolutionary relationships of vertebrate lactate dehydrogenase isozymes A_4 (muscle), B_4 (heart), and C_4 (testis). J. Biol. Chem. 258:7029–7032, 1983.
50. Schlatter, D., Kriech, O., Suter, F., Zuber, H. Structure and function of L-lactate dehydrogenase from thermophilic, mesophilic and psychrophilic bacteria, VIII. The primary structure of the psychrophilic lactate dehydrogenase from *Bacillus psychrosaccharolyticus*. Biol. Chem. Hoppe Seyler 368:1435–1446, 1987.
51. Stangl, D., Wiederkehr, F., Suter, F., Zuber, H. Structure and function of L-lactate dehydrogenases from thermophilic and mesophilic bacteria, V. The complete amino-acid sequence of the mesophilic L-lactate dehydrogenase from *Bacillus megaterium*. Biol. Chem. Hoppe Seyler 368: 1157–1166, 1987.
52. Chandrasekhar, K., McPherson, A., Jr., Adams, M.J., Rossmann, M.G. Conformation of coenzyme fragments when bound to lactate dehydrogenase. J. Mol. Biol. 76: 503–518, 1973.
53. Kabsch, W., Sander, C. Dictionary of protein secondary structure: Pattern recognition of hydrogen-bonded and geometrical features. Biopolymers 22:2577–2637, 1983.
54. Rao, S.T., Rossmann, M.G. Comparison of super-secondary structures in proteins. J. Mol. Biol. 76:241–256, 1973.
55. Rossmann, M.G., Argos, P. Exploring structural homology of proteins. J. Mol. Biol. 105:75–95, 1976.
56. Atkinson, T., Barstow, D.A., Chia, W.N., Clarke, A.R., Hart, K.W., Waldman, A.D.B., Wigley, D.B., Wilks, H., Holbrook, J.J. Mapping motion in large proteins by single tryptophan probes inserted by site-directed mutagenesis: Lactate dehydrogenase. Biochem. Soc. Trans. 15:991–993, 1987.
57. Rossmann, M.G., Liljas, A., Brändén, C.I., Banaszak, L.J. Evolutionary and structural relationships among dehydrogenases. In: "The Enzymes," 3rd edn., Vol. XI. Boyer, P.D. (ed.). New York: Academic Press, 1975:61–102.
58. Eklund, H., Samama, J.P., Jones, T.A. Crystallographic investigations of nicotinamide adenine dinucleotide binding to horse liver alcohol dehydrogenase. Biochemistry 23: 5982–5996, 1984.
59. Reddy, B.S., Saenger, W., Mühlegger, K., Weimann, G. Crystal and molecular structure of the lithium salt of nicotinamide adenine dinucleotide dihydrate (NAD^+, DPN^+, cozymase, codehydrase I). J. Am. Chem. Soc. 103:907–914, 1981.
60. Gronenborn, A.M., Clore, G.M. Conformation of NAD^+ bound to yeast and horse liver alcohol dehydrogenase in solution. The use of the proton-proton transferred nuclear Overhauser enhancement. J. Mol. Biol. 157:155–160, 1982.
61. Adams, M.J., Liljas, A., Rossmann, M.G. Functional anion binding sites in dogfish M_4 lactate dehydrogenase. J. Mol. Biol. 76:519–531, 1973.
62. Narendra, N., Seshadri, T.P., Viswamitra, M.A. Structure of trisodium fructose 1,6-diphosphate octahydrate, $3Na^+.\ C_6H_{11}O_{12}P_2^{3-}.8H_2O$. Acta Crystallogr. C41:31–34, 1985.